Shear-assisted grain coarsening in colloidal polycrystals

Wei Li[a], Yi Peng[b], Yongjun Zhang[c], Tim Still[d], A. G. Yodh[d], and Yilong Han[a,1]

[a]Department of Physics, Hong Kong University of Science and Technology, Clear Water Bay, Kowloon, Hong Kong 999077, China; [b]Beijing National Laboratory for Condensed Matter Physics, Institute of Physics, Chinese Academy of Sciences, Beijing 100190, China; [c]Key Laboratory of Functional Polymer Materials, State Key Laboratory of Medicinal Chemical Biology, Institute of Polymer Chemistry, College of Chemistry, Nankai University, Tianjin 300071, China; and [d]Department of Physics and Astronomy, University of Pennsylvania, Philadelphia, PA 19104

Edited by David A. Weitz, Harvard University, Cambridge, MA, and approved August 23, 2020 (received for review June 28, 2020)

Grain growth under shear annealing is crucial for controlling the properties of polycrystalline materials. However, their microscopic kinetics are not well understood because individual atomic trajectories are difficult to track. Here, we study grain growth with single-particle kinetics in colloidal polycrystals using video microscopy. Rich grain-growth phenomena are revealed in three shear regimes, including the normal grain growth (NGG) in weak shear melting–recrystallization process in strong shear. For intermediate shear, early stage NGG is arrested by built-up stress and eventually gives way to dynamic abnormal grain growth (DAGG). We find that DAGG occurs via a melting–recrystallization process, which naturally explains the puzzling stress drop at the onset of DAGG in metals. Moreover, we visualize that grain boundary (GB) migration is coupled with shear via disconnection gliding. The disconnection-gliding dynamics and the collective motions of ambient particles are resolved. We also observed that grain rotation can violate the conventional relation $R \times \theta =$ constant (R is the grain radius, and θ is the misorientation angle between two grains) by emission and annihilation of dislocations across the grain, resulting in a step-by-step rotation. Besides grain growth, we discover a result in shear-induced melting: The melting volume fraction varies sinusoidally on the angle mismatch between the triangular lattice orientation of the grain and the shear direction. These discoveries hold potential to inform microstructure engineering of polycrystalline materials.

colloidal crystal | shear-coupled grain boundary migration | grain rotation | dynamic abnormal grain growth | melting–recrystallization

Polycrystals, such as metals, rocks, ceramics, and ice, exist widely in nature and have broad applications in industry. Generally, polycrystals are composed of small crystalline patches, or grains, embedded within a network of grain boundaries (GBs). GB networks dominate polycrystal microstructure and material properties. Thus, GB engineering, based on controlling grain growth and manipulating GB kinetics, plays a key role in materials processing (1–3). Despite its importance, however, GB kinetics remain poorly understood at the single-particle level because atomic motions, especially motions of GBs buried in the bulk solid, are difficult to track using electron microscopy and other scattering techniques.

Mechanical or thermal annealing leads to coalescence of polycrystalline grains. This phenomenon, known as grain growth, is governed by GB kinetics. Growing grains induce stresses on and experience complex interactions with nearby grains and defects. There are two types of grain growth: normal grain growth (NGG) and abnormal grain growth (AGG). In NGG, the microstructure evolves in a uniform manner; grain size is log-normally distributed, and mean grain size exhibits power-law growth. Traditional NGG theory describes GBs like a soap froth dominated by surface tension; it predicts that the mean grain diameter (d) grows with time (t), according to $d(t) \sim t^{\alpha}$ with $\alpha = 0.5$. To date, experimentally measured α values are always less than 0.5 due, for example, to stress effects from grain growth (4), impurities (5), temperature (6), external fields (7), and other factors (8, 9). Moreover, this curvature-driven growth theory fails to explain observed GB dynamics, such as stress-assisted grain growth (10, 11), grain rotation (12, 13), and AGG (14, 15). Indeed, multiple grain-growth mechanisms may contribute concurrently (9) to produce more complicated growth behaviors.

Most studies of GB migration during NGG focus on GB curvature effects (9, 16). GB motion is generally coupled with tangential motion, wherein the geometrical constraints of two adjacent lattices cause the two grains to slide tangentially relative to one another as the GB migrates in the direction normal to its surface (17). This mechanism, called GB shear coupling (18), has been observed in a macroscopic experiment in aluminum, but lacks corroborating microscopic observations (11). Shear-coupled GB migration arises from gliding of disconnections (17, 19), but disconnection kinetics, including its effect on the ambient lattice, have not been experimentally observed. The recent experiment in gold bicrystals provides the first observation of GB migration associated with the displacements of disconnections, but its electron microscopy cannot track their motions and the shear displacement (20). In fact, a direct link between microscopic dynamics and the collective behavior of the many thousands of atoms that constitute the GB and surrounding grains has not yet been made and represents a serious challenge for both experiment and theory (2).

Significance

Grain growth and grain-boundary motions during shear play key roles in polycrystal annealing. Notably, complex interactions between neighboring grains give rise to nontrivial grain-boundary kinetics that are not well understood, in part because electron microscopy cannot dynamically track atoms. Here, we observe grain-growth behaviors and elucidate kinetics from experiments with colloidal polycrystals that resolve single-particle motions; the observations reveal shear-coupled grain-boundary migration, grain rotation via emission of dislocations across the grain, melting-point shifts for different lattice orientations, and melting–recrystallization phenomena, which provide a mechanism for unexplained dynamic abnormal grain growth. These fundamental findings are critical results for understanding and processing polycrystalline materials.

Author contributions: W.L. and Y.H. designed research; W.L. performed research; Y.P., Y.Z., and T.S. contributed new reagents/analytic tools; W.L. analyzed data; and W.L., A.G.Y., and Y.H. wrote the paper.

The authors declare no competing interest.

This article is a PNAS Direct Submission.

[1]To whom correspondence may be addressed. Email: yilong@ust.hk.

This article contains supporting information online at https://www.pnas.org/lookup/suppl/doi:10.1073/pnas.2013456117/-/DCSupplemental.

First published September 16, 2020.

AGG is a "discontinuous" phenomenon, wherein one or more grains grow extremely rapidly, resulting in huge grains surrounded by a uniform (i.e., log-normally distributed) microstructure of much smaller grains (14, 15). When AGG arises in dynamic annealing conditions—e.g., under the influence of shear forces—it is referred to as dynamic AGG (DAGG). DAGG was first discovered in molybdenum sheets in 2009, wherein it proved to be an effective technique to produce large single crystals (21). All of the experiments observed a sudden stress drop at the onset of DAGG (21–23), but the central mechanisms of DAGG and the stress drop remain unclear.

Here, we experimentally explore these phenomena using colloidal solids. Colloids are excellent model systems for study of GB kinetics because the micrometer-sized particles and their thermal motions can be directly visualized and tracked by optical microscopy inside bulk crystals and polycrystals (24–29). In fact, colloid experiments have already provided useful insights about grain growth (5, 8, 9), GB roughening (30–32), GB kinetics (16, 33), and quasi-localized phonons associated with GBs (34). Previous studies focused on grain size distributions, dopant effects, roughening, and curvature-driven grain growth. Here, by contrast, we study shear-coupled GB migration due to disconnection kinetics, grain rotations via rapid cross-grain dislocation gliding and annihilation, and transient melting–recrystallization behavior in DAGG. The first two phenomena were studied in metals, but early investigations lacked microscopic experimental observations; study of the third phenomenon has not been explored before.

Results

Experiment. The colloidal polycrystals used in our experiment are composed of thermally sensitive poly(*N*-isopropylacrylamide) (NIPA) microgel spheres sealed in a $40 \times 5 \times 0.02\text{-mm}^3$ glass channel (*SI Appendix*, Fig. S1). The diameter of these NIPA spheres, σ, changed linearly from 1.04 μm at 25°C to 0.89 μm at 30°C in water (24, 35). The spheres have short-range repulsive interparticle interactions and display hard-sphere-like phase behaviors. Here, we slightly rescaled their effective diameter so that the melting volume fraction, $\phi_m = 0.545$, was the same as hard spheres. In our experiments, the volume fraction ϕ plays a role similar to that of inverse temperature in atomic systems (28). Since NIPA spheres are more than 90% water, their refractive index is very close to that of water, and the (111) planes in the bulk crystal were clearly imaged by bright-field microscopy.

The NIPA spheres self-assembled into a face-centered cubic polycrystalline thin film consisting of ~ 25 layers. The (111) planes of all grains were parallel with the top/bottom sample cell walls due to flow annealing when the colloid was injected into the sample. The quasi-two-dimensional (quasi-2D) nature of these polycrystals is apparent because different layers had the same GB network and exhibited similar growth behaviors when sheared (columnar grains in Movie S6). Our 2D imaging cannot track the motions of dislocations whose Burgers vectors are out of plane, but these dislocations are much less common than dislocations with Burger vectors in the xy plane—i.e., because of the columnar nature of the GB network. A syringe pump exerted oscillatory compression on the sample with shear strain amplitude γ_m and a period of 2.4 s (*SI Appendix*, Fig. S1 *A* and *C*). The shear strain was uniform in the z direction at the center of the bulk polycrystalline film (*SI Appendix*, Fig. S1*D*), and the flow speed was uniform in the xy plane (Movie S1). Particle motions were recorded at 18 frames per s with a charge-coupled device camera. Particles were tracked in the 2D slice by standard image-analysis techniques (36); full three-dimensional (3D) positions were not measured. More experimental details are given in *Materials and Methods* and *SI Appendix*.

Four types of grain growth arose during annealing, depending on strain amplitude (γ_m): NGG for $0 \le \gamma_m < 0.05$; early stage NGG and late-stage DAGG for $0.05 < \gamma_m < 0.50$; melting and recrystallization for $0.50 < \gamma_m \lesssim 2.00$; and melting for $\gamma_m \ge 2.00$. The four regimes reported in detail herein were measured at $\phi = 0.593$; nevertheless, the reported effects are robust, occurring for different ϕ with regime boundaries slightly shifted.

$0 \le \gamma_m < 0.05$: NGG. We first considered the small shear regime ($0 \le \gamma_m < 0.05$), wherein grains coalesced in the freshly made polycrystal exhibiting NGG, as shown in Fig. 1. The grains are colored by mismatch angle Θ between the shear (along the x axis) and the [1 0] lattice orientation. We used the bond-orientational correlation length d as the mean grain diameter (*SI Appendix*, Fig. S2) (9). The collapse of the orientational correlation functions in *SI Appendix*, Fig. S2*D* reflects a self-similar microstructure during the grain growth, a signature of NGG. The NGG grain growth obeyed a power law with exponent $\alpha = 0.2$ (Fig. 1*D*); since it was less than 0.5, we surmised that stress was building up during grain growth and that this stress effectively reduced the growth rate (11, 17, 37).

From the videos of NGG, we observed shear-coupled GB migration and its associated disconnection gliding. A disconnection is a topological line defect constrained on a GB with a step component h and a dislocation component with Burgers vector **b**, denoted by $(\mathbf{b}, h)$ (Fig. 1*E*). Disconnection gliding along the tangential direction of the GB effectively displaced the GB in a direction normal to the GB by distance H. Such shear-coupled GB motion was observed in a macroscopic experiment that tracked the displacement of a scratch mark on a metal plate (11). The in situ transmission electron microscopy (20) can resolve the displacement of disconnection, but cannot track the reference atoms (e.g., red particles in Fig. 1 *F–I*) and, thus, is not able to measure the shear displacement and shear coupling factor B/H in Fig. 1*I*.

Fig. 1 *F–I* shows that when a GB propagates along its normal direction with a displacement H, the two grains have a relative shear displacement $B = \beta H$ along the tangential direction, where the constant $\beta = 0.70$ is the shear coupling factor (17). We found that the whole NGG process was dominated by such shear-coupled GB migrations via disconnection gliding. Previous simulations showed that multilayer disconnections [e.g., disconnection (1+2+3) in Fig. 1*G*] have lower energy than the sum of corresponding single-layer disconnections (20); we found that the multilayer disconnections were less mobile and tended to decompose into single-layer disconnections when gliding across the red reference line (Fig. 1 *F–I*). Any plastic rearrangement in a crystal can be understood as a result of dislocations' motions. Here, the GB propagated via the motion of disconnections—i.e., rows of dislocations in the z direction. Of course, not all kinetics are captured by dislocation motions—e.g., several atoms swapping positions in a closed loop without changing structure. Generally, electron microscopy can track the dislocation displacement, but it is not fast enough to resolve the individual atomical motions that accompany such displacements. Here, we further found that disconnection gliding induced stresses and triggered cooperative string-like motions of particles in the ambient crystalline grains (*SI Appendix*, Fig. S5 and Movie S3). The chain of cooperative motions was longer when disconnections moved faster under stronger shear. Note that cooperative motions also occurred outside the GB to relax stress when the GB was moving.

$0.05 < \gamma_m < 0.50$: Three Stages. When $0.05 < \gamma_m < 0.50$, the grain growth proceeded in three stages, as shown in Fig. 2*A*. In stage I (Fig. 2 *B* and *C*), $d \propto t^{0.2}$ (Fig. 2*A*), as was the case for NGG when $\gamma_m < 0.05$. In stage II, the grain growth

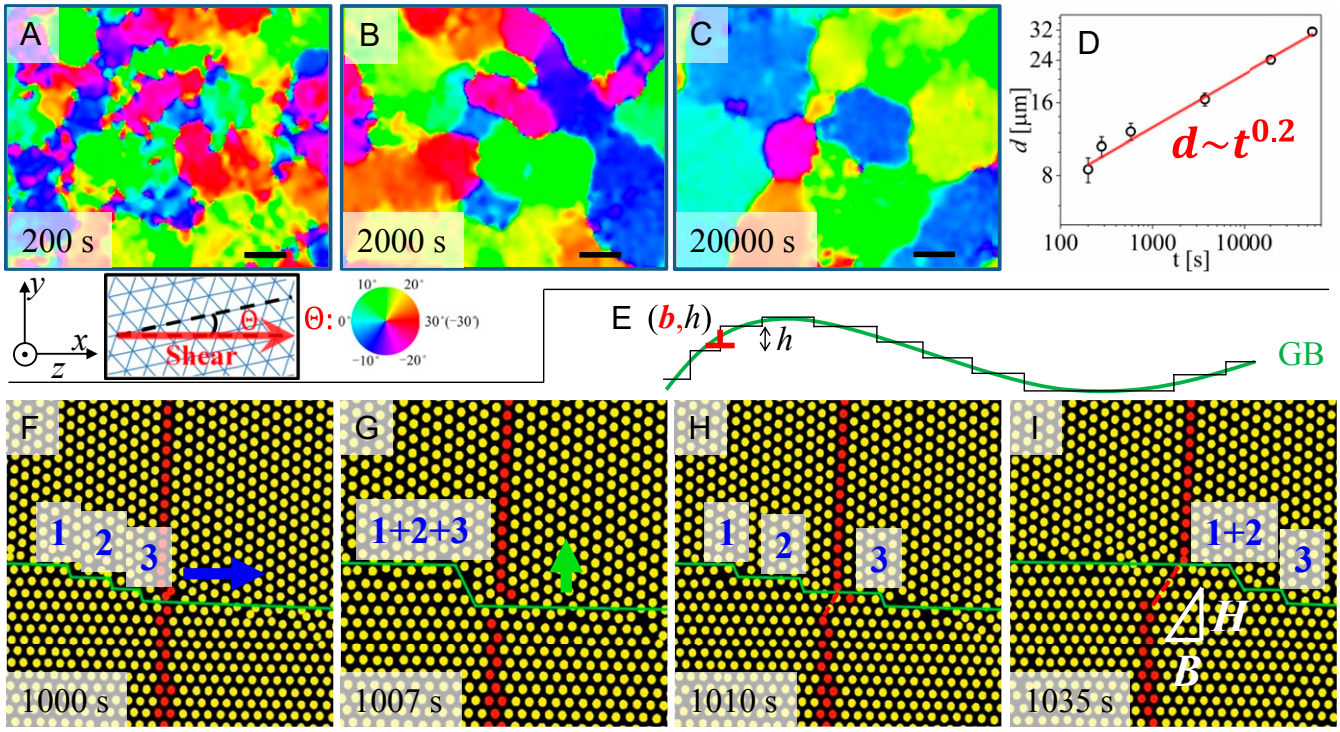

Fig. 1. NGG in a sample with no applied shear ($\gamma_m = 0$). (*A*–*C*) The grain growth at $t = 200$ s, 2,000 s, and 20,000 s, respectively. The focal plane is defined as the *xy* plane. Colors represent the mismatch angle Θ between the shear (along the *x* axis) and local lattice orientation (i.e., the [1 0] orientation of the triangular lattice); *Inset* and color wheel below *A* and *B*. (Scale bars: 20 μm.) This sample was rapidly quenched from a liquid state at $\phi = 0.488$ to $\phi = 0.593$ at $t = 0$ s, and it became fully crystallized within 200 s. (*D*) The mean grain diameter in the sample depicted in *A*–*C* grows according to a power law with exponent $\alpha = 0.2$. (*E*) A curved GB can be decomposed into many flat GB segments connected by disconnections. (*F*–*I*) A GB (green curve) migrates via disconnection gliding (Movie S2). (*F*) At t = 1,000 s, disconnections 1, 2, and 3 on the left side of the red reference line are moving to the right (blue arrow) along the GB. (*G*) At t = 1,007 s, the three disconnections combine to form a larger one. (*H*) At t = 1,010 s, the larger disconnection breaks up into three smaller ones. Disconnection 3 crossed the red reference line and created a gap in it. (*I*) At t = 1,035 s, disconnections 1 and 2 also cross the red reference line, and the gap (red dashed line) in the red reference line is widened. The shear displacement, *B*, results in a GB migration displacement, *H*, in the direction normal to the GB interface.

became stagnant, and then the grains started to melt (Fig. 2*D*). In stage III, the melted grains recrystallized from the unmelted crystals; this effect led to very fast grain growth (Fig. 2 *E* and *F*). The duration of the three stages is sensitive to γ_m. Stage I became shorter at larger γ_m, and it vanished for $\gamma_m > 0.50$ (Fig. 2*A*, *Inset*).

In stage I, grains not only grow or shrink, but also rotate. Grain rotation is a natural consequence of the shear-coupled GB migration (38, 39). Briefly, to ameliorate complex geometrical constraints imposed by the multiple neighboring grains, the phenomenon of grain rotation has usually been studied for cylindrical grains fully embedded within another grain in quasi-2D

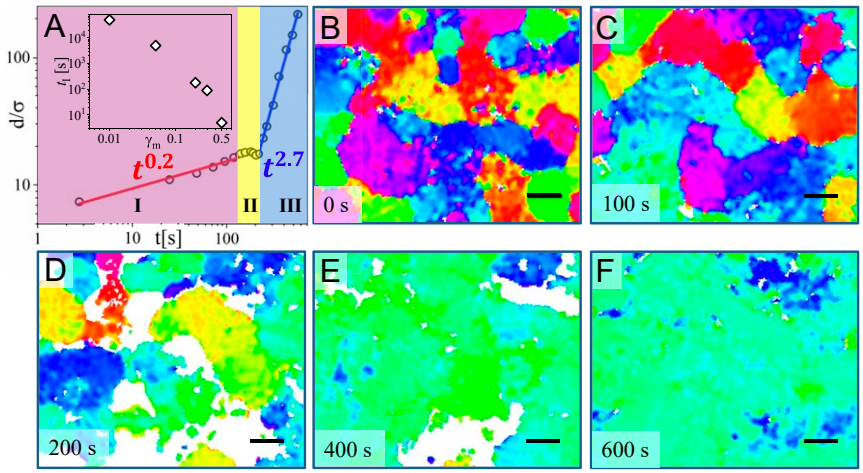

Fig. 2. Polycrystal annealing under oscillatory shear with $\gamma_m = 0.20$. (*A*) The mean grain diameter grows in three stages. (*A*, *Inset*) Stage I becomes shorter as γ_m increases. (*B*–*F*) Coarsening of the polycrystal colored according to the color wheel in Fig. 1. Liquid regions are labeled in white. (Scale bars: 20 μm.)

samples (18, 33, 40). Shrinkage of the grain requires that the GB migrates toward its center, which, in turn, creates a collective shear displacement relative to the outer grain that drives rotation. An example of resulting rotation is shown in Fig. 3*A*. Since a GB can be viewed as a chain of dislocations, and since the number of such topological defects is conserved (i.e., when they have no chance to annihilate/generate, which is usually the case), the grain radius R and the misorientation angle θ should satisfy the equation (18, 38, 40):

$$R\theta = \text{constant}. \qquad [1]$$

To date, Eq. **1** has been observed in the rotation grains with small misorientation angle ($\theta < 10^\circ$) relative to the ambient lattice and in the early stages of rotation grains with a large misorientation angle (33, 38, 40). In practice, grains that have large-angle GBs typically rotate to a certain magic angle with a low GB energy, but the rotation usually stops before the angle is reached because of repulsions between neighboring dislocations on the GB (41).

Eq. **1** breaks down when dislocations on the GB can annihilate, and Srinivasan and Cahn (41) have noted that annihilation should occur only between dislocations with opposite Burgers vectors located on opposite GBs. Dislocations inside a rotating grain surrounded by multiple grains have been observed in metals (42, 43), but the kinetics and annihilation of these dislocations were not able to be resolved by electron microscopy (41). While simulations have revealed the breakdown of Eq. **1**, they could not resolve rapid dislocation gliding through the grain; thus, the mechanisms remain unclear (40). Here, the slow dynamics of colloidal particles enable us to visualize rapid dislocation-annihilation kinetics and experimentally confirm Srinivasan and Cahn's picture of the dislocation-annihilation mechanism. For example, the upper GB in Fig. 3*C* emits two [0 1] dislocations, which glided through the grain and annihilated another two dislocations at the lower GB. This behavior triggered subsequent emission of a [0 $\bar{1}$] dislocation from the lower GB toward the upper GB, as shown in Fig. 3*D*.

Usually, two dislocations annihilate each other completely when their Burgers vectors point in opposite directions. Occasionally, two dislocations without oppositely directed Burgers vectors can partly annihilate, as shown in Fig. 3 *C* and *D*, *Inset* (e.g., [1 $\bar{1}$] + [0 1] = [1 0]). One or two dislocations gliding through the grain (e.g., Fig. 3 *C* and *D*) can be viewed as a small-angle GB cutting through the grain and thereby rotating part of the grain by a small angle (e.g., 1.5° in Fig. 3*C*). Such small rotations were repeated several times until θ decreased from 30° to 16° (Fig. 3 *D* and *E*). After this point, the GB disintegrated and left a small disordered region (Fig. 3*E*), wherein individual dislocations could barely be resolved. Such disordered regions slowly annealed into a single crystal (Fig. 3*F*). We further found that a higher shear effectively promoted rapid dislocation gliding and grain rotation.

During stage II (Fig. 2*A*), grains stopped growing due to the stress that had accumulated in stage I. Such stagnation effects have been intensively studied (17, 44), but subsequent melting and recrystallization have never been reported. When shear flow occurs along the lattice orientation, different layers in the z direction can easily slide against each other and maintain the lattice structure. By contrast, a shear flow perpendicular to the lattice orientation causes "bumping" with neighboring layers during sliding, resulting in more stress and possible grain melting. A simple example of such case is given in *SI Appendix*, Fig. S3 and Movie S5. To quantify the melting volume fraction, $\phi_m(\Theta)$, of grains with different Θ, we measured the maximum lattice angle, Θ_m, of the unmelted grains at $\gamma_m = 0.50$ (Fig. 4). Note that, here, we chose this high γ_m because the melting started immediately after the shear was applied without the initial NGG stage (Fig. 4*B*).

Fig. 4*D* shows that ϕ_m linearly decreased with $\cos(6\Theta_m)$; the factor 6 arose from the sixfold lattice symmetry. We observed that applied shear expanded the liquid–crystal coexistence regime from $0.494 < \phi < 0.545$ (no shear) (28) to $0.519 < \phi < 0.595$ (Fig. 4*D*), which generalized the equilibrium phase diagram of hard spheres (no shear) to the case with shear. The melting point $\phi_{m0} = 0.545$ shifted more than the freezing point $\phi_{f0} = 0.494$, indicating that the shear promotes melting more

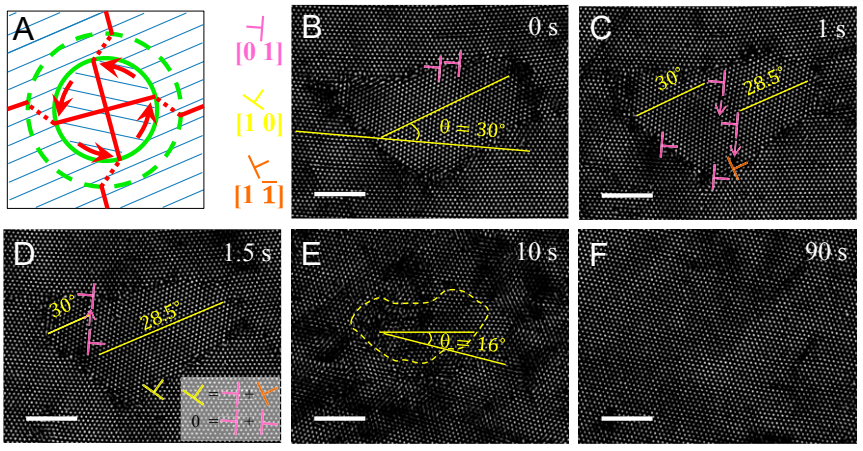

Fig. 3. Rotation of a grain fully embedded in another grain ($\gamma_m = 0.20$). (*A*) Decreasing the radius *R* leads to an increase in the misorientation angle θ, as required by Eq. **1**. The solid and dashed red lines are reference lines and gaps, similarly shown in Fig. 1 *H* and *I*. This relationship breaks down when dislocations can annihilate each other—e.g., *B*–*E* and Movie S4. (*B*) A grain with a misorientation angle $\theta = 30^\circ$ fully embedded in a large crystal. (*C*) At $t = 1$ s, two [0 1] dislocations (⊥) in *B* emitted from the upper GB move downward and annihilate with two dislocations at the lower GB. Such annihilation induces a slight rotation of the right half of the grain, resulting in a new grain-orientation angle of $\theta = 28.5^\circ$. The dislocations are labeled in color (see key between *A* and *B*). The detailed distributions of dislocations in *B* and *C* are shown in *SI Appendix*, Fig. S6. The left bottom dislocation will be emitted through the grain in *D*. (*D*) At $t = 1.5$ s, the lower GB emits a [0 $\bar{1}$] dislocation toward the upper GB; this causes the middle region to rotate and the region oriented at 28.5° to grow larger. (*E*) After the emission and annihilation of several other dislocations, a disordered region with an average $\theta = 16^\circ$ remains. (*F*) The disordered region completely merges with the ambient lattice at $t = 90$ s. (Scale bars: 10 μm.)

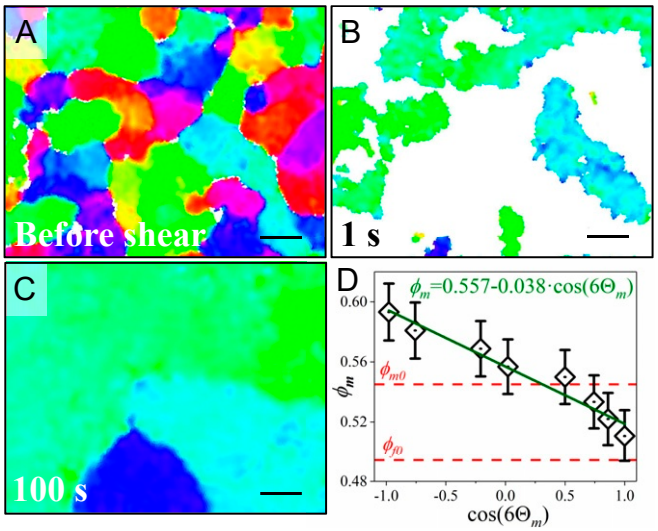

Fig. 4. Melting and recrystallization at $\gamma_m = 0.50$. (Scale bars: 20 μm.) (*A*) Polycrystal with $\phi = 0.55$ before shear was applied; see the color wheel in Fig. 1. (*B*) The crystal melted immediately, 1 s after the shear was applied. Liquid regions are in white. (*C*) At $t = 100$ s, the polycrystal recrystallized and formed small-Θ grains. (*D*) Melting-volume fraction ϕ_m for grains with different Θ. The red dashed lines label melting and freezing volume fractions of a hard-sphere system with no shear, corresponding to 0% and 100% liquid, respectively.

when the system is more of a crystal than a liquid. Although the shift and expansion of the liquid–crystal coexistence regime varied under different γ_m, we found that the relationship, $\phi_m \sim \cos(6\Theta_m)$, was robust for different γ_m. Such a result is qualitatively expected and has been qualitatively observed in plasma crystals—e.g., grains with $\Theta = 30^\circ$ melt more easily than grains with $\Theta = 0^\circ$ (45).

In stage III, the melted region recrystallized from the surface of the unmelted small-Θ grains, resulting in a rapid increase in the mean grain size—i.e., DAGG (Fig. 2 *A*, *E*, and *F*). Evidently, the unmelted crystals serve as large postcritical nuclei, from which grains grow much faster than via the GB migrations characteristic of most polycrystal annealing processes. Previously, DAGG has been observed in metals (21, 23, 46), but the underling mechanism remains unknown. A major puzzle, for example, concerns why the onset of DAGG is always associated with a sudden stress drop (21, 23, 46). Our observations of the melting–recrystallization process suggest that partial melting can effectively relax the stresses that had accumulated during stage I.

$\gamma_m > 0.50$: Shear Melting. For $0.5 < \gamma_m \lesssim 2.00$, the stages I and II (NGG and stagnation) vanish, and grain growth is purely a DAGG process. All of the crystalline grains with a mismatch angle larger than a particular Θ_m were found to melt in a few seconds after shear was applied (Fig. S7 *A* and *B*), and this Θ_m decreased to 0° (i.e., all grains melted) when $\gamma_m \gtrsim 1.00$. At extremely large shear ($\gamma_m > 2.00$), the polycrystal melted catastrophically without recrystallization.

Conclusions

Colloidal crystals are much softer than atomic crystals, and, with them, we can easily study a broad range of strains that reveal rich grain-growth phenomenology and GB kinetics with single-particle resolution in bulk polycrystals under shear. Importantly, the shear-induced grain-growth behaviors in colloidal and atomic systems should share some similarities, because γ is a dimensionless quantity, and because colloidal particles and some metallic atoms can be approximately modeled as hard spheres (47). In a different vein, the conditions (γ) in our colloid experiments share similarities with olivine, the main component of the Earth's upper mantle. Olivine relaxes into a preferred grain orientation along the shear at $0.5 \lesssim \gamma \lesssim 2$, produces amorphous patches at $2 \lesssim \gamma \lesssim 5$, and becomes an amorphous solid at $\gamma \gtrsim 5$ (48). After the shear is removed, olivine maintains its amorphous structure, whereas the colloidal sphere sample recrystallizes. This difference could be due to their varied interactions: Olivine molecules have strong attractive and anisotropic bonds, whereas colloidal spheres exhibit isotropic repulsion, which can easily induce crystallization.

We observed universal bond-orientational correlations during the evolution of NGG (*SI Appendix*, Fig. S2*D*), and grain growth exhibited a constant exponent $\alpha = 0.2$ at different γ_m (Figs. 1*D* and 2*A*), suggesting that grain growth is determined by the same coarsening mechanism (i.e., shear-coupled GB migration) rather than external forces. Our experiment provides an observation of shear-coupled GB migration at the single-particle level and confirms its underlying mechanism of disconnection gliding with stress relaxation via string-like motions in the ambient crystal (*SI Appendix*, Fig. S5).

Grain rotation is one basic type of annealing phenomenon, but its kinetics is not well understood. We observed a scenario that grain rotates step by step, and each step corresponds to the dislocation gliding across the grain and annihilating at the opposite GB. This scenario is promoted by oscillatory shear, provided that the grain is small enough for the dislocations on opposite sides to attract each other. Thus, when the mean grain radius decreases, we expect that the polycrystal will become unstable because many dislocations can attract and annihilate each other.

Moreover, we observed DAGG in colloidal crystals. DAGG has been observed in various alloys, but its mechanism is unclear. We found that the DAGG arises from a melting–recrystallization process. This observation can also explain the puzzle of the sudden stress drop found at the onset of DAGG in metals (21–23).

Besides the above results about grain growth and GB motion, we discovered a result in shear-induced melting: $\phi_m \sim \cos(6\Theta)$. This finding is consistent with a qualitative observation in plasma crystals that the lattice is easily distorted when its orientation is perpendicular to the direction of shear (45). Similarly, we conjecture that the melting point changes linearly with $\cos(m\Theta)$ for a lattice with m-fold symmetry in the plane perpendicular to shear strain. Schemes based on this idea provide a way to tailor the grain orientation and remove unwanted grains by melting and recrystallization under appropriate shear.

Materials and Methods

We synthesized NIPA (also known as pNIPA or pNIPAM) microgel spheres with less than 3% polydispersity and dispersed them in an aqueous buffer solution with 1 mM acetic acid (24). The NIPA spheres were slightly negatively charged; they exhibited short-range steric repulsion, and their effective diameter, σ, varied linearly with temperature. Note that the diameter of these soft spheres is ambiguous. Here, we assigned $\sigma(T)$ from measurements based on image analysis. We then rescaled the diameter slightly so that the melting volume fraction of the 3D crystal was the same as that of hard spheres, $\phi_m = 0.545$. By using this rescaled diameter, the measured freezing point of our sample is $\phi_f = 0.49$, which is very close to that of hard spheres (0.494). Hence, NIPA spheres exhibited almost the same phase behavior as hard spheres. The channel fabrication and oscillatory shear are shown in *SI Appendix*.

Data Availability. All study data are included in the article and *SI Appendix*.

ACKNOWLEDGMENTS. We thank Xian Chen and Yang Xiang for helpful discussions. This work was supported by Research Grants Council's General Research Fund Grants 16302518 and 16302720; NSF Grants DMR16-07378 and Materials Research Science and Engineering Centers DMR-1720530.

1. T. Watanabe, S. Tsurekawa, The control of brittleness and development of desirable mechanical properties in polycrystalline systems by grain boundary engineering. *Acta Mater.* **47**, 4171–4185 (1999).
2. J. Han, S. L. Thomas, D. J. Srolovitz, Grain-boundary kinetics: A unified approach. *Prog. Mater. Sci.* **98**, 386–476 (2018).
3. S. Gokhale, K. H. Nagamanasa, R. Ganapathy, A. Sood, Grain growth and grain boundary dynamics in colloidal polycrystals. *Soft Matter* **9**, 6634–6644 (2013).
4. C. V. Thompson, R. Carel, Stress and grain growth in thin films. *J. Mech. Phys. Solid.* **44**, 657–673 (1996).
5. K. Yoshizawa, T. Okuzono, T. Koga, T. Taniji, J. Yamanaka, Exclusion of impurity particles during grain growth in charged colloidal crystals. *Langmuir* **27**, 13420–13427 (2011).
6. W. Liu, Y. Wu, J. He, T. Nieh, Z. Lu, Grain growth and the Hall–Petch relationship in a high-entropy FeCrNiCoMn alloy. *Scr. Mater.* **68**, 526–529 (2013).
7. T. Palberg, W. Mönch, J. Schwarz, P. Leiderer, Grain size control in polycrystalline colloidal solids. *J. Chem. Phys.* **102**, 5082–5087 (1995).
8. C. Harrison *et al.*, Mechanisms of ordering in striped patterns. *Science* **290**, 1558–1560 (2000).
9. F. A. Lavergne, D. G. Aarts, R. P. Dullens, Anomalous grain growth in a polycrystalline monolayer of colloidal hard spheres. *Phys. Rev. X* **7**, 041064 (2017).
10. K. Zhang, J. Weertman, J. Eastman, Rapid stress-driven grain coarsening in nanocrystalline Cu at ambient and cryogenic temperatures. *Appl. Phys. Lett.* **87**, 061921 (2005).
11. T. Gorkaya, D. A. Molodov, G. Gottstein, Stress-driven migration of symmetrical $< 1\,0\,0 >$ tilt grain boundaries in A bicrystals. *Acta Mater.* **57**, 5396–5405 (2009).
12. E. Ma, Watching the nanograins roll. *Science* **305**, 623–624 (2004).
13. Z. Shan *et al.*, Grain boundary-mediated plasticity in nanocrystalline nickel. *Science* **305**, 654–657 (2004).
14. J. B. Koo, D. Y. Yoon, M. F. Henry, The effect of small deformation on abnormal grain growth in bulk Cu. *Metall. Mater. Trans. A* **33**, 3803–3815 (2002).
15. T. Kusama *et al.*, Ultra-large single crystals by abnormal grain growth. *Nat. Commun.* **8** , 354 (2017).
16. Q. Wei, X. Wu, Grain boundary dynamics under mechanical annealing in two-dimensional colloids. *Phys. Rev. E* **70**, 020401 (2004).
17. S. L. Thomas, K. Chen, J. Han, P. K. Purohit, D. J. Srolovitz, Reconciling grain growth and shear-coupled grain boundary migration. *Nat. Commun.* **8**, 1764 (2017).
18. J. W. Cahn, J. E. Taylor, A unified approach to motion of grain boundaries, relative tangential translation along grain boundaries, and grain rotation. *Acta Mater.* **52**, 4887–4898 (2004).
19. L. Zhang, J. Han, Y. Xiang, D. J. Srolovitz, Equation of motion for a grain boundary. *Phys. Rev. Lett.* **119**, 246101 (2017).
20. Q. Zhu *et al.*, In situ atomistic observation of disconnection-mediated grain boundary migration. *Nat. Commun.* **10**, 156 (2019).
21. J. Ciulik, E. Taleff, Dynamic abnormal grain growth: A new method to produce single crystals. *Scr. Mater.* **61**, 895–898 (2009).
22. D. L. Worthington, N. A. Pedrazas, P. J. Noell, E. M. Taleff, Dynamic abnormal grain growth in molybdenum. *Metall. Mater. Trans.A.* **44**, 5025–5038 (2013).
23. P. J. Noell, D. L. Worthington, E. M. Taleff, The initiation and propagation of dynamic abnormal grain growth in molybdenum. *Metall. Mater. Trans. A* **46**, 5708–5718 (2015).
24. A. M. Alsayed, M. F. Islam, J. Zhang, P. J. Collings, A. G. Yodh, Premelting at defects within bulk colloidal crystals. *Science* **309**, 1207–1210 (2005).
25. S. Suresh, Crystal deformation: Colloid model for atoms. *Nat. Mater.* **5**, 253–254 (2006).
26. P. Schall, D. A. Weitz, F. Spaepen, Structural rearrangements that govern flow in colloidal glasses. *Science* **318**, 1895–1899 (2007).
27. R. Ganapathy, M. R. Buckley, S. J. Gerbode, I. Cohen, Direct measurements of island growth and step-edge barriers in colloidal epitaxy. *Science* **327**, 445–448 (2010).
28. B. Li, D. Zhou, Y. Han, Assembly and phase transitions of colloidal crystals. *Nat. Rev. Mater.* **1**, 15011 (2016).
29. K. H. Nagamanasa, S. Gokhale, R. Ganapathy, A. Sood, Confined glassy dynamics at grain boundaries in colloidal crystals. *Proc. Natl. Acad. Sci. U.S.A.* **108**, 11323–11326 (2011).
30. S. Gokhale, K. H. Nagamanasa, V. Santhosh, A. Sood, R. Ganapathy, Directional grain growth from anisotropic kinetic roughening of grain boundaries in sheared colloidal crystals. *Proc. Natl. Acad. Sci. U.S.A.* **109**, 20314–20319 (2012).
31. T. O. Skinner, D. G. Aarts, R. P. Dullens, Grain-boundary fluctuations in two-dimensional colloidal crystals. *Phys. Rev. Lett.* **105**, 168301 (2010).
32. M. Liao, X. Xiao, S. T. Chui, Y. Han, Grain-boundary roughening in colloidal crystals. *Phys. Rev. X* **8**, 021045 (2018).
33. F. A. Lavergne, A. Curran, D. G. Aarts, R. P. Dullens, Dislocation-controlled formation and kinetics of grain boundary loops in two-dimensional crystals. *Proc. Natl. Acad. Sci. U.S.A.* **115**, 6922–6927 (2018).
34. K. Chen *et al.*, Phonons in two-dimensional soft colloidal crystals. *Phys. Rev. E* **88**, 022315 (2013).
35. P. J. Yunker *et al.*, Physics in ordered and disordered colloidal matter composed of poly(*N*-isopropylacrylamide) microgel particles. *Rep. Prog. Phys.* **77**, 056601 (2014).
36. J. C. Crocker, D. G. Grier, Methods of digital video microscopy for colloidal studies. *J. Colloid Interface Sci.* **179**, 298–310 (1996).
37. M. Legros, D. S. Gianola, K. J. Hemker, In situ TEM observations of fast grain-boundary motion in stressed nanocrystalline aluminum films. *Acta Mater.* **56**, 3380–3393 (2008).
38. A. Adland, Y. Xu, A. Karma, Unified theoretical framework for polycrystalline pattern evolution. *Phys. Rev. Lett.* **110**, 265504 (2013).
39. A. Haslam, S. Phillpot, D. Wolf, D. Moldovan, H. Gleiter, Mechanisms of grain growth in nanocrystalline fcc metals by molecular-dynamics simulation. *Mater. Sci. Eng. A* **318**, 293–312 (2001).
40. Z. Trautt, Y. Mishin, Grain boundary migration and grain rotation studied by molecular dynamics. *Acta Mater.* **60**, 2407–2424 (2012).
41. S. Srinivasan, J. Cahn, Challenging some free-energy reduction criteria for grain growth. *Sci. Technol. Interface*, 1–14 (2002).
42. L. Wang *et al.*, Grain rotation mediated by grain boundary dislocations in nanocrystalline platinum. *Nat. Commun.* **5**, 4402 (2014).
43. L. Wang *et al.*, In situ observation of stress induced grain boundary migration in nanocrystalline gold. *Scr. Mater.* **134**, 95–99 (2017).
44. E. A. Holm, S. M. Foiles, How grain growth stops: A mechanism for grain-growth stagnation in pure materials. *Science* **328**, 1138–1141 (2010).
45. V. Nosenko, A. Ivlev, G. Morfill, Anisotropic shear melting and recrystallization of a two-dimensional complex plasma. *Phys. Rev. E* **87**, 043115 (2013).
46. E. M. Taleff, N. A. Pedrazas, A new route for growing large grains in metals. *Science* **341**, 1461–1462 (2013).
47. C. Xia *et al.*, Origin of noncubic scaling law in disordered granular packing. *Phys. Rev. Lett.* **118**, 238002 (2017).
48. M. Bystricky, K. Kunze, L. Burlini, J. P. Burg, High shear strain of olivine aggregates: Rheological and seismic consequences. *Science* **290**, 1564–1567 (2000).